Strong Photoluminescence Enhancement of MoS_2 through Defect Engineering and Oxygen Bonding

Haiyan Nan,[†,¶] Zilu Wang,[†,¶] Wenhui Wang,[†] Zheng Liang,[‡] Yan Lu,[§] Qian Chen,[†] Daowei He,[⊥] Pingheng Tan,[§] Feng Miao,[∥] Xinran Wang,[⊥] Jinlan Wang,[†,*] and Zhenhua Ni[†,*]

[†]Department of Physics, Southeast University, Nanjing 211189, China, [‡]Graphene Research and Characterization Center, Taizhou Sunano New Energy Co., Ltd., Taizhou 225300, China, [§]State Key Laboratory for Superlattices and Microstructures, Institute of Semiconductors, Chinese Academy of Sciences, Beijing 100083, China, [⊥]National Laboratory of Solid State Microstructures, Jiangsu Provincial Key Laboratory of Advanced Photonic and Electronic Materials, School of Electronic Science and Engineering, Nanjing University, Nanjing 210093, China, and [∥]National Laboratory of Solid State Microstructures, School of Physics, Nanjing University, Nanjing 210093, China. [¶]These authors contributed equally to this work.

ABSTRACT We report on a strong photoluminescence (PL) enhancement of monolayer MoS_2 through defect engineering and oxygen bonding. Micro-PL and Raman images clearly reveal that the PL enhancement occurs at cracks/defects formed during high-temperature annealing. The PL enhancement at crack/defect sites could be as high as thousands of times after considering the laser spot size. The main reasons of such huge PL enhancement include the following: (1) the oxygen chemical adsorption induced heavy p doping and the conversion from trion to exciton; (2) the suppression of nonradiative recombination of excitons at defect sites, which was verified by low-temperature PL measurements. First-principle calculations reveal a strong binding energy of ~2.395 eV for an oxygen molecule adsorbed on a S vacancy of MoS_2. The chemically adsorbed oxygen also provides a much more effective charge transfer (0.997 electrons per O_2) compared to physically adsorbed oxygen on an ideal MoS_2 surface. We also demonstrate that the defect engineering and oxygen bonding could be easily realized by mild oxygen plasma irradiation. X-ray photoelectron spectroscopy further confirms the formation of Mo—O bonding. Our results provide a new route for modulating the optical properties of two-dimensional semiconductors. The strong and stable PL from defects sites of MoS_2 may have promising applications in optoelectronic devices.

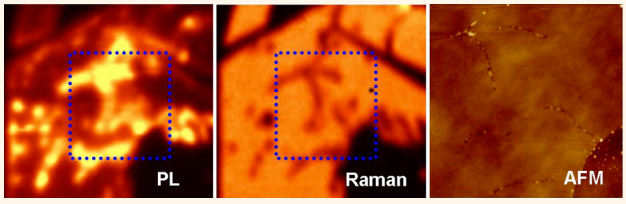

KEYWORDS: MoS_2 · photoluminescence · defect engineering · plasma · oxygen bonding · excitons

There is a great need for controlling the properties of two-dimensional (2D) materials to fulfill the requirements of various applications. For example, modulating the electrical and optical properties of graphene through electrical and magnetic fields,[1] strain,[2] stacking geometry,[3] edge chirality,[4] and defects[5] has been successfully demonstrated.[6] Defects such as vacancies are active centers for molecular adsorption and chemical functionalization, which would provide a great platform for the interplay between 2D materials and various atoms and molecules. Among the most investigated 2D layered materials, single-layer and multilayer molybdenum disulfide (MoS_2) are semiconductors with direct/indirect band gap of ~1.2—1.8 eV,[7,8] which makes them promising candidates for optoelectronic applications, such as photodetectors,[9,10] photovoltaics,[11—13] and light emitters.[14] However, the photoluminescence (PL) of as-prepared monolayer MoS_2 has lagged behind expectation for a high-quality direct band gap semiconductor.[8,15] Previous work has shown that the weak PL is mostly due to formation of negatively charged excitons (also named as negative trions) in the naturally n-doped MoS_2.[16] The switch from trion to exciton in MoS_2 *via* electrical gating and molecular adsorptions (*e.g.*, O_2, H_2O, TCNQ) can dramatically enhance the PL of MoS_2.[16—19] Structural defects, such as vacancies, dislocations, grain boundaries, and edges have been observed in both pristine/as-grown MoS_2[20—22] and electron beam/plasma-irradiated samples.[23,24] The proper utilization of these defects to improve the optical properties of MoS_2 is highly desirable.

In this work, we present the defect engineering of monolayer MoS_2 and the

* Address correspondence to zhni@seu.edu.cn, jlwang@seu.edu.cn.

Received for review January 27, 2014 and accepted May 16, 2014.

Published online May 16, 2014
10.1021/nn500532f

strong oxygen bonding on the defect sites. The PL intensities at the defect sites could be enhanced by at least thousands of times, as observed by high-resolution micro-PL images. The oxygen adsorbed on the defect site has very strong bonding energy and would introduce heavy p doping in MoS_2 and hence a conversion from trion to exciton. The excitons at defects sites are dominated by radiative recombination at room temperature, resulting in a high PL quantum efficiency. We also show that the defect engineering could be easily realized by oxygen plasma irradiation.

RESULTS AND DISCUSSION

Figure 1a shows a PL intensity image of an as-prepared monolayer MoS_2, which is very uniform across the whole sample. The PL spectrum from location A is shown by the black curve in Figure 1g, with a relatively weak peak located at ~1.79 eV, corresponding to the direct band gap emission. The PL intensity is enhanced by 6-fold (Figure 1b) after the sample is annealed for 1 h at 350 °C in vacuum (0.1 Pa) and exposed to ambient air. At the same time, the PL peak blue shifts to ~1.81 eV, as shown by the green curve in Figure 1g. These phenomena have been reported and explained by the physical adsorption of O_2 and H_2O molecules on MoS_2 (p-type doping, with O_2 as the dominant contributor).[18] The as-prepared MoS_2 is normally n-doped, due to the presence of defects or substrate unintentional doping.[20,25] In such cases, the photoexcited electron–hole pairs would bind with excess electrons to form negative trions (labeled as X^-, with lower energy), instead of neutral excitons (labeled as X, with higher energy). The depletion of excess electrons by O_2/H_2O adsorption can therefore switch the dominant PL process from trion recombination to exciton recombination. The physically adsorbed molecules are not stable due to the weak binding energy and can be easily removed by vacuum pumping. Figure 1c shows that the PL intensity almost reduces to its original value after pumped down to 0.1 Pa. On the other hand, the results are quite different for the sample annealed at higher temperature. Figure 1d–f shows the PL intensity images of another monolayer MoS_2 after similar annealing and pumping processes, but with a higher annealing temperature of 500 °C. As shown in Figure 1e, the PL image becomes highly inhomogeneous after annealing. In some locations (*e.g.*, C and D), the PL intensities are dramatically increased to 30 and 89 times, respectively, as compared to its original values. Furthermore, the PL intensities from those locations only drop slightly (to 22 and 80 times, respectively) after the pumping process (Figure 1f,h), and they are very stable after laser irradiation of ~30 min with a power of ~0.5 mW. This suggests that,

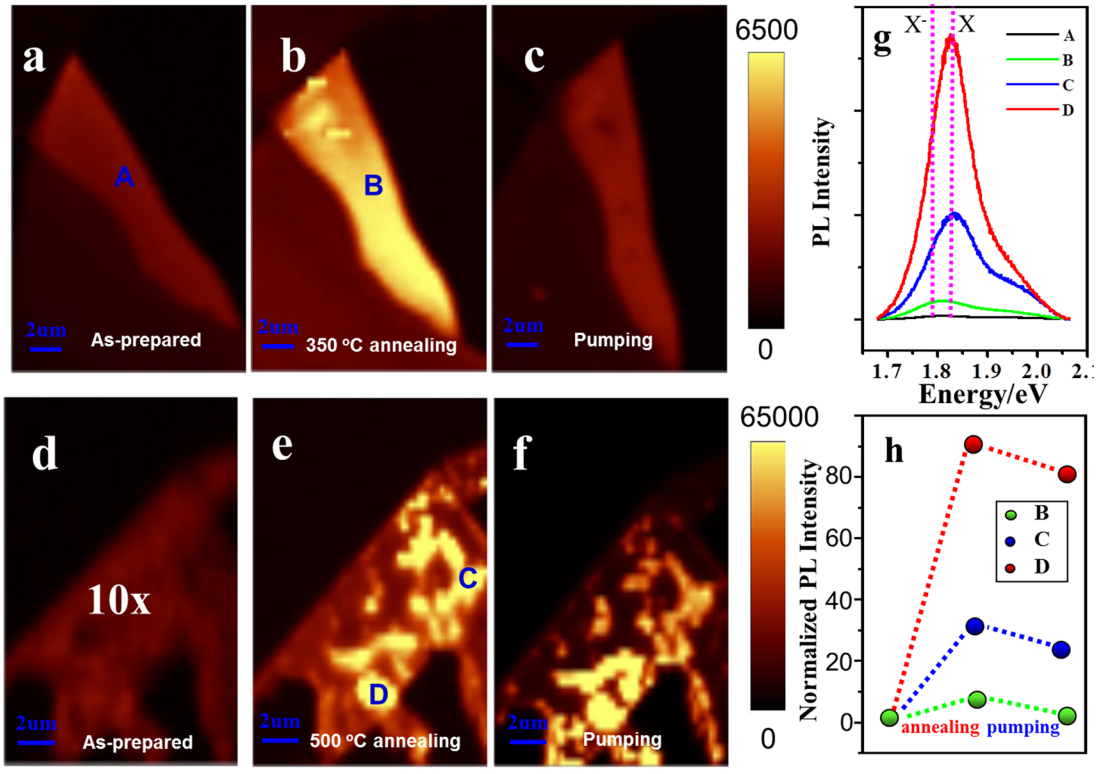

Figure 1. PL intensity images of monolayer MoS_2: (a) as-prepared, (b) annealed in vacuum for 1 h at 350 °C, (c) after pumped down to 0.1 Pa. The images have the same color bar; PL intensity images of another monolayer MoS_2: (d) as-prepared, (e) annealed in vacuum for 1 h at 500 °C, (f) after pumped down to 0.1 Pa. The images have the same color bar; (g) PL spectra taken from locations A–D in the images; (h) change of normalized PL intensities (as compared to the original values) of locations B–D throughout the annealing and pumping process.

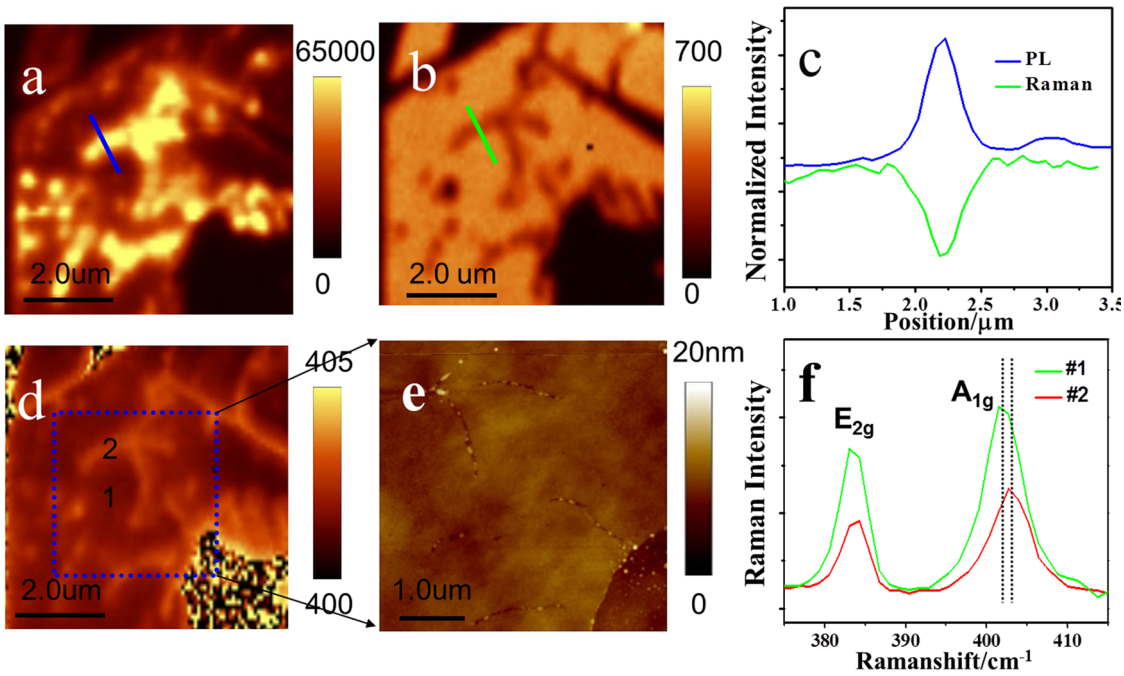

Figure 2. PL (a) and Raman A_{1g} peak (b) intensity images of monolayer MoS_2 after annealed for 1 h at 500 °C. (c) Normalized intensity profiles of a crack in (a) and (b); (d) Raman image of the A_{1g} peak frequency; (e) AFM image corresponding to the blue square in (d); (f) Raman spectra taken from locations #1 and #2 in (d).

in these locations, there is a strong interaction between MoS_2 and adsorbed molecules, possibly with a chemical adsorption.

In order to have a more detailed investigation, high-resolution micro-PL and Raman images, as well as atomic force microscope (AFM) image, are taken from a selected region of the second sample. Figure 2a,b presents PL and Raman (A_{1g} peak) intensity images, where the fine structures can be distinguished with a high spatial resolution of ~300 nm. As can be seen, there is a very good correlation between the PL and Raman intensity images, with higher PL intensities in lower Raman intensity regions. AFM investigation in Figure 2e further reveals that these regions are exactly corresponding to the cracks in MoS_2, which are formed during the high-temperature annealing. The origin of the formation of cracks will be discussed later. We also observe a clear blue shift of the MoS_2 A_{1g} peak in the cracked regions, as shown in Figure 2d. Raman spectroscopy is a powerful tool to study the properties of MoS_2.[26,27] A p/n-type doping would cause a blue shift/red shift of A_{1g} peak of MoS_2 due to the change of electron−phonon interactions, while the E_{2g} peak frequency is almost unaffected.[28,29] The A_{1g} peak of the cracked region is slightly blue-shifted by ~1 cm^{-1} as compared to other regions (Figure 2f), which suggests that there is a p-type doping. It could be understood as follows: Mo and S atoms at the cracks of MoS_2 contain numerous dangling bonds, which can be considered as a lot of defects and are very active centers for molecular adsorption. Therefore, O_2 can adsorb on the cracks/defects with much stronger binding energy as well as introduce p-type doping, as compared to the ideal MoS_2 surface. This is also supported by first-principle calculations in the later sections. The p-type doping would introduce a conversion from trion to exciton emissions, as verified by the blue shift of PL peak in Figure 1g (from ~1.79 eV (X^-) of as-prepared sample to ~1.83 eV (X) of cracked regions). The intensity profiles of PL and Raman images across a crack are shown in Figure 2c. Both of these two curves can be well fitted by Gaussian functions. As the width of the crack is only around 30 nm, the width of the Raman intensity profile of ~300 nm is only limited by the spatial resolution of the system. The PL intensity profile has a similar width of ~304 nm, which suggests that the PL signals are mainly from the cracked regions. In viewing of this, the PL enhancement at cracks/defects regions should be re-estimated by considering the laser spot size. In a normal microscope setup, the PL signals are collected from the whole regions of spot size, that is, ~300 nm in our case. The PL signals from cracks/defects with nanometer sizes are ~30 times stronger compared to the original PL intensity collected from the whole ~300 nm spot size regions! By considering the cracks as two one-dimensional edges with effective widths of several nanometers, this would give a PL enhancement of at least thousands of times at the crack/defect sites. Such a huge PL enhancement cannot be simply explained by the switch of PL process from trion recombination to exciton recombination, which can only enhance the PL intensities by several to tens of times.[16−19] We suggest that this is related to the high PL quantum efficiency of excitons at defect sites.

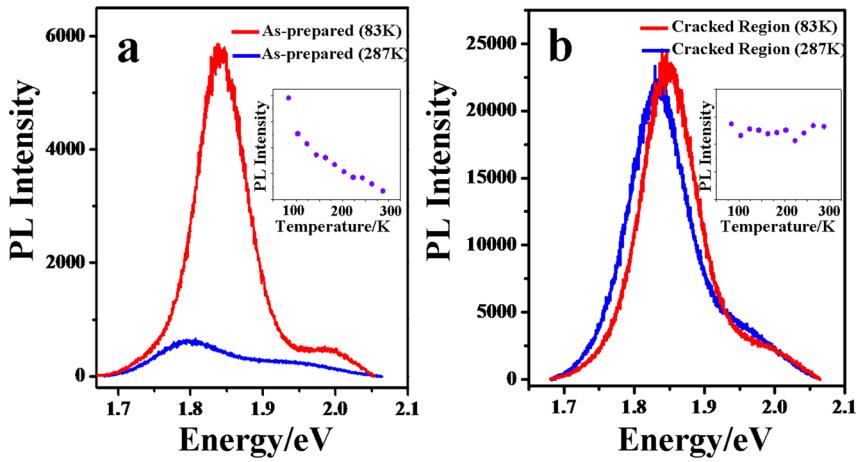

Figure 3. PL spectra of (a) as-prepared monolayer MoS_2 and (b) cracked regions in annealed MoS_2, taken at 83 and 287 K. The changes of PL intensities with the change of temperatures (287−83 K) are shown in the insets.

Low-temperature PL measurements are carried out and shown in Figure 3. The PL spectra from as-prepared monolayer MoS_2 as well as cracked regions (similar to locations C and D in Figure 1e) are collected at temperatures from 83 to 287 K in a low-temperature Linkam stage (with 1 °C temperature accuracy and stability). The temperature dependence of PL intensity can be expressed by[30,31]

$$I_{PL}(T) = I_0 \times k_{rad}(T)/(k_{rad}(T) + k_{nonrad}(T)) \quad (1)$$

where I_0 is the maximum PL intensity at very low temperature, and $k_{rad}(T)$ and $k_{nonrad}(T)$ are the temperature-dependent radiative and nonradiative recombination rates. The nonradiative recombination rates k_{nonrad} contain the rates of defect trapping k_{relax} and electron relaxation within the conduction and valence band k_{relax}.[8] In most of the materials, the PL intensities as well as quantum efficiency dramatically decrease as the temperature increases, due to the thermally activated nonradiative recombination. The PL intensity of as-prepared MoS_2 is reduced to ~10% with the increase of temperature from 83 to 287 K (Figure 3a and inset) because of nonradiative recombination. Surprisingly, the PL intensity of cracked regions is almost unchanged with the change of temperature (Figure 3b and inset). According to eq 1, the nonradiative recombination rate k_{nonrad} of the excitons at cracked regions is almost negligible, and the PL process is dominated by radiative recombination.[32] This could be the main reason for huge PL enhancement at defect/crack sites. The excitons in lower-dimensional systems (in our case, the excitons may localize at the defect sites) generally have much larger binding energy,[33,34] which may suppress the thermally activated nonradiative recombination including defect trapping and result in a very high PL quantum efficiency. Previous work also found that the thermal activation energy (temperature) for nonradiative recombination increases with the decrease of quantum well thickness, due to the stronger quantum confinement effect.[35] Further work on the time-resolved PL experiments to investigate the recombination process of these localized excitons would be very interesting. Recently, a strong PL enhancement at WS_2 edges has also been reported and was attributed to the exciton accumulation or localized excitons near lattice defects (different structure and chemical composition of the platelet edges). [36] The PL enhancement did not happen at WS_2 edges created *via* mechanical scratch, which suggests that it might be due to the W−O bonding formed during the growth of WS_2 at high temperature since the raw material is WO_3.

We have also checked the origin of crack formation and oxygen bonding by changing the vacuum pressure in the annealing chamber. As can be seen in Supporting Information Figure S1a, annealing at 10^{-4} Pa at 600 °C does not introduce oxygen bonding, indicated by the recovery of PL intensity to its original value after vacuum pumping. There are no cracks formed either. However, if we change the vacuum pressure to 100 Pa (which means there are certain amounts of oxygen in the chamber at 600 °C), a stronger PL enhancement is observed and the PL intensity only decreases by ~50% after vacuum pumping. This suggests that oxygen in the chamber plays an important role in the formation of cracks and oxygen bonding. We also anneal the sample at ~300 °C in air and observe the formation of triangle pits in MoS_2, which is similar to the results reported in ref 37. There is also a strong PL enhancement as can be seen in Figure S1b. Therefore, it is suggested that the cracks in our sample are formed by reaction of O_2 (due to the not very high vacuum condition) with MoS_2 at high temperature, followed by the chemical bonding of an oxygen molecule at the crack edges at high temperature.

The binding energy as well as charge transfer between O_2 molecule and MoS_2 is calculated by first-principles methods. Previous experimental and theoretical

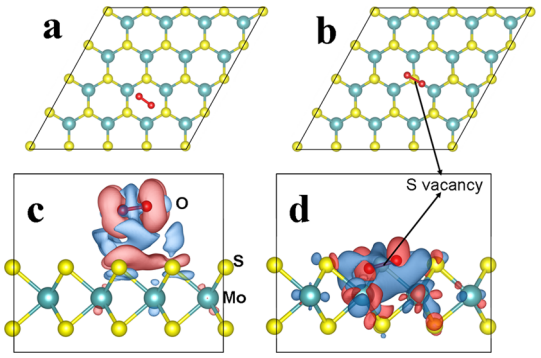

Figure 4. Relaxed configuration and charge density difference of an O_2 molecule physisorbed on perfect monolayer MoS_2 (a,c) and chemisorbed on defective monolayer MoS_2 containing a monosulfur vacancy (b,d). The positive and negative charges are shown in red and blue, respectively. Isosurface values are 3×10^{-4} and 1×10^{-2} $e/Å^3$ for (c) and (d), respectively.

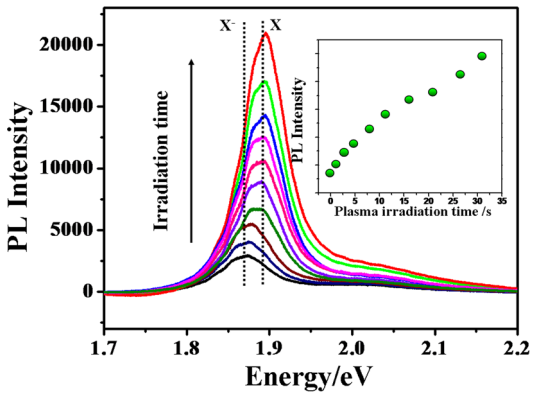

Figure 5. PL spectra of monolayer MoS_2 after oxygen plasma irradiation with different durations. The change of PL intensities with plasma irradiation times is shown in the inset.

results have shown that monosulfur vacancies are the most stable defective structures,[21] and therefore our simulation is focused on a monosulfur vacancy on the MoS_2 lattice. The structures of the O_2 molecule adsorbed on an ideal 4×4 supercell of monolayer MoS_2 and the same supercell in the presence of a S vacancy are shown in Figure 4a,b, respectively. The binding energy between the O_2 molecule and an ideal MoS_2 is only 0.102 eV and therefore can be considered as physical adsorption. In contrast, the binding energy of an O_2 molecule on a S vacancy of MoS_2 is 2.395 eV. This suggests that the O_2 molecule on the S vacancy of MoS_2 can be considered as chemisorbed and therefore is very stable under vacuum pumping. We have calculated the energy barrier between physical and chemical adsorption of oxygen molecules on the MoS_2 vacancy and found a reaction barrier of ~1.05 eV, which can be easily overcome under high-temperature annealing conditions. Details can be found in Supporting Information Figure S2. The charge transfer between an O_2 molecule and ideal MoS_2 (physical adsorption) is only 0.021e (from MoS_2 to oxygen), while that between an O_2 molecule and S vacancy (chemical adsorption) reaches 0.997e (from MoS_2 to oxygen). The increase of charge transfer between oxygen and MoS_2 with S vacancy is also one of the reasons for the huge PL enhancement at cracked regions. It should be noted that the charge transfer is strongly localized at the defect site (Figure 4d), which means that the defect can be treated as a hole localization center.[38] The binding of free electrons or trions with such localized holes would form localized excitons, which are very stable and could even avoid nonradiative recombination. This would be the main reason of huge PL enhancement at defect/crack sites of MoS_2.

Since the PL enhancement occurs at the defect sites, controlling the defect concentration (especially S vacancies) and introducing oxygen adsorption can be a promising method for manipulating the optical properties of MoS_2. Here we adopt mild oxygen plasma (13.56 MHz, 5 W, 5 Pa) irradiation to controllably introduce defects in MoS_2. It has been reported that plasma irradiation can easily introduce S vacancies in MoS_2.[23,24] At the same time, the oxygen ions are more reactive and can easily interact with MoS_2 at the defect sites. As shown in Figure 5 and inset, the PL intensity increases gradually with the increase of plasma irradiation time. By careful control of experimental conditions, the PL enhancement could be as high as 100 times. As the power of oxygen plasma is very weak, it can hardly introduce damage to MoS_2, which is verified by the almost unchanged Raman line shapes (see Figure S3). The PL intensities of plasma-irradiated MoS_2 only drops by ~10−20% under vacuum pumping and even after 1 h annealing at 400 °C, indicating a strong oxygen chemical adsorption.

X-ray photoelectron spectroscopy (XPS) is used to study the change of MoS_2 structure after annealing and oxygen plasma treatment. Here, a bulk sample is used due to the experimental limitations. The XPS spectra of as-prepared, 350 °C annealed, and oxygen plasma treated (13.56 MHz, 5 W, 5 Pa, 30 s) MoS_2 are shown in Figure 6. All of the samples contain the characteristic peaks of MoS_2, with a doublet Mo^{4+} $3d_{3/2}$ and Mo^{4+} $3d_{5/2}$ at ~232.6 and ~229.4 eV, and a S 2s peak at binding energies of ~226.4 eV (Figure 6a).[39] The XPS spectra of as-prepared and 350 °C annealed sample are similar, but with a slightly stronger O 1s peak located at ~532 eV for the annealed sample (Figure 6b). This should be due to the physically adsorbed oxygen molecules. In the oxygen plasma treated sample, a well-pronounced peak at ~236.2 eV shows up. This peak is attributed to the Mo^{6+} state, which is also a doublet but with one of the peaks overlapping with Mo^{4+} $3d_{3/2}$ at ~233 eV.[40] At the same time, Mo^{4+} and S 2s peaks are reduced. In addition, the intensity of the O 1s peak increases dramatically after oxygen plasma treatment (Figure 6b). The appearance of higher

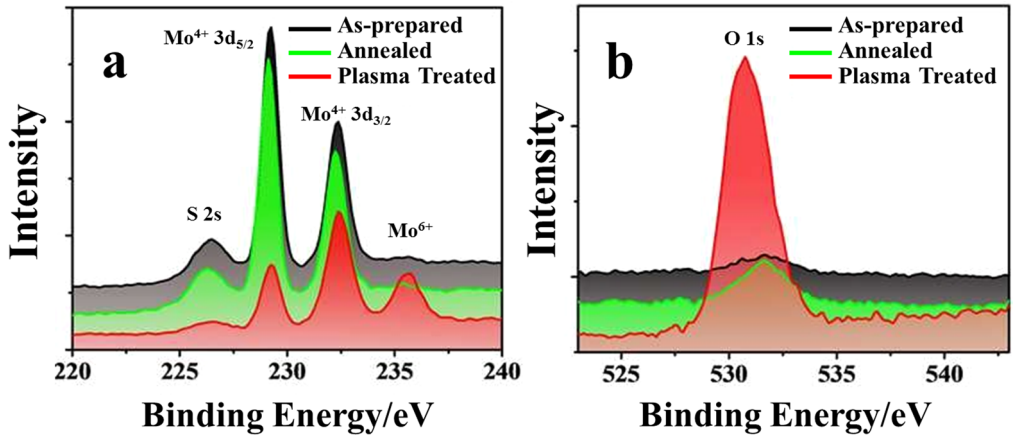

Figure 6. XPS spectra of (a) Mo 3d and S 2s core levels and (b) O 1s binding energy region measured from as-prepared, annealed at 350 °C for 1 h, and oxygen plasma treated MoS_2.

oxidized Mo^{6+} states and the strongly increased oxygen concentration in plasma treated MoS_2 are clear signatures of the formation of Mo−O bonds.[40] There might be MoO_3 formed after oxygen plasma treatment. However, MoO_3 does not present obvious PL signals and therefore does not contribute to the strong PL enhancement.

Finally, it should be noted that vacancy defects in MoS_2 would introduce localized donor states inside the band gap of MoS_2, and low carrier density transport is dominated by hopping *via* these localized gap states.[20] However, it seems that certain amounts of defects in MoS_2 generated by thermal annealing and plasma treatment would not degrade its optical properties, while providing the possibility of defect engineering through chemical bonding with oxygen or other types of molecule.

CONCLUSION

To summarize, we have achieved a strong PL enhancement of MoS_2 through defect engineering and oxygen bonding. The micro-PL and Raman images clearly reveal that the PL enhancement occurs at the defect sites and can be as high as thousands-fold after considering the laser spot size. Such a huge PL enhancement is attributed to oxygen bonding induced heavy p doping as well as high quantum efficiency of excitons localized at defect sites. Finally, we adopt oxygen plasma to controllably introduce defects and oxygen bonding in MoS_2, resulting in a controllable manipulation of PL. Our results provide a new route to modulate the optical properties of MoS_2. The strong PL of MoS_2 achieved by defect engineering would be very promising for optoelectronic applications, such as light-emitting devices. [41]

EXPERIMENTAL METHODS

Sample Preparation, Thermal Annealing, and Vacuum Pumping. Monolayer MoS_2 flakes are exfoliated from bulk crystals (SPI Supplies) and transferred to a Si wafer with a 300 nm SiO_2 capping layer. The thickness of monolayer MoS_2 is confirmed by Raman spectra, optical contrast, and AFM.[15] The samples are annealed at the temperature of 350 or 500 °C for 1 h in a quartz tube with pressure of 0.1 Pa. After being annealed, the samples are taken out and studied by PL/Raman measurements. The pumping treatment is performed in a homemade vacuum chamber with a pressure of 0.1 Pa, which can be put under the Raman microscope.

Micro-PL/Raman, AFM, and XPS Measurements. Micro-Raman/PL measurements are carried out using a Witec alpha 300R confocal Raman system. A 100× objective lens with numerical aperture (NA) of 0.9 is used in the Raman and PL experiments, and the spot size of a 532 nm laser is estimated to be ~300 nm using a scanning edge method.[42] The excitation source is 532 nm laser (2.33 eV) with a laser power below 0.5 mW to avoid laser-induced sample damage. For PL and Raman images, the sample is placed on an $x-y$ piezostage and scanned under the illumination of a laser with a step size of 100 nm. The PL and Raman spectra from every spot of the sample are recorded. Data analysis is done by using WITec Project 2.10 software. AFM is carried out using a Nanoscape 8.15 system with tapping mode. XPS (ULVAC-PHI PHI5000) equipped with a monochromatic Al Kα (1486.7 eV) X-ray source is used to scrutinize the MoS_2 surface.

Density Functional Theory Calculations. Spin-polarized density functional theory calculations are performed by employing the van der Waals density functional[43] within the framework of plane-wave pseudopotential method, which is implemented in the Vienna ab initio simulation package (VASP).[44] The optB86b-vdW exchange functional[45] is used for the vdW correction since its estimated lattice constant for MoS_2 is closest to the experimental value (3.16 Å) in our calculations. A large spacing of 15 Å between adjacent single layers is used to prevent interlayer interactions. A plane-wave basis set with kinetic energy cutoff of 400 eV is used. The Brillouin zone is sampled by $5 \times 5 \times 1$ k-point meshes within the Monkhorst−Pack scheme.[46] All atomic positions are optimized until the maximum Hellmann−Feynman forces acting on each atom is less than 0.01 eV/Å.

Conflict of Interest: The authors declare no competing financial interest.

Acknowledgment. This work is supported by NSFC (11104026, 11274154, 11225421, 61376104, 21173040, 21373045, 61325020, 61261160499), Program for New Century Excellent Talents in

University (NCET-11-0094), NBRP (2013CBA01600, 2011CB302004, and 2010CB923401), the open research fund of State Key Laboratory of Advanced Optical Communication Systems and Networks, SJTU, China and Natural Science Foundation of Jiangsu Province (BK2011585, BE2011159, BK20130016). We would like to thank Weiwei Zhao, Yumeng You, Da Zhan, Chuanhong Jin, and Xing Wu for their help on this work and computational resources at SEU and National Supercomputing Center in Tianjin.

Supporting Information Available: Additional figures and details as described in the text. This material is available free of charge *via* the Internet at http://pubs.acs.org.

REFERENCES AND NOTES

1. Zhang, Y.; Tang, T. T.; Girit, C.; Hao, Z.; Martin, M. C.; Zettl, A.; Crommie, M. F.; Shen, Y. R.; Wang, F. Direct Observation of a Widely Tunable Bandgap in Bilayer Graphene. *Nature* **2009**, *459*, 820–823.
2. Ni, Z. H.; Yu, T.; Luo, Z. Q.; Wang, Y. Y.; Liu, L.; Wong, C. P.; Miao, J. M.; Huang, W.; Shen, Z. X. Probing Charged Impurities in Suspended Graphene Using Raman Spectroscopy. *ACS Nano* **2009**, *3*, 569–574.
3. Yan, W.; He, W. Y.; Chu, Z. D.; Liu, M.; Meng, L.; Dou, R. F.; Zhang, Y. F; Liu, Z. F.; Nie, J. C.; He, L. Strain and Curvature Induced Evolution of Electronic Band Structures in Twisted Graphene Bilayer. *Nat. Commun.* **2013**, *4*, 3159.
4. Xu, Y. N.; Zhan, D.; Liu, L.; Suo, H.; Ni, Z. H.; Nguyen, T. T.; Zhao, C.; Shen, Z. X. Thermal Dynamics of Graphene Edges Investigated by Polarized Raman Spectroscopy. *ACS Nano* **2010**, *5*, 147–152.
5. Ni, Z. H.; Ponomarenko, L. A.; Nair, R. R.; Yang, R.; Anissimova, S.; Grigorieva, I. V.; Schedin, F.; Blake, P.; Shen, Z. X.; Hill, E. H.; *et al.* On Resonant Scatterers as a Factor Limiting Carrier Mobility in Graphene. *Nano Lett.* **2010**, *10*, 3868–3872.
6. Zhan, D.; Yan, J. X.; Lai, L. F.; Ni, Z. H.; Liu, L.; Shen, Z. X. Engineering the Electronic Structure of Graphene. *Adv. Mater.* **2012**, *24*, 4055–4069.
7. Mak, K.; Lee, C.; Hone, J.; Shan, J.; Heinz, T. F. Atomically Thin MoS_2: A New Direct-Gap Semiconductor. *Phys. Rev. Lett.* **2010**, *105*, 136805.
8. Splendiani, A.; Sun, L.; Zhang, Y.; Li, T.; Kim, J.; Chim, C. Y.; Galli, G.; Wang, F. Emerging Photoluminescence in Monolayer MoS_2. *Nano Lett.* **2010**, *10*, 1271–1275.
9. Yin, Z. Y.; Li, H.; Li, H.; Jiang, L.; Shi, Y. M.; Sun, Y. H.; Lu, G.; Zhang, Q.; Zhang, H. Single-Layer MoS_2 Phototransistors. *ACS Nano* **2011**, *6*, 74–80.
10. Lee, H. S.; Min, S. W.; Chang, Y. G.; Park, M. K.; Nam, T.; Kim, H.; Kim, J. H.; Ryu, S.; Im, S. MoS_2 Nanosheet Phototransistors with Thickness-Modulated Optical Energy Gap. *Nano Lett.* **2012**, *12*, 3695–3700.
11. Feng, J.; Qian, X. F.; Huang, C. W.; Li, J. Strain-Engineered Artificial Atom as a Broad-Spectrum Solar Energy Funnel. *Nat. Photonics* **2012**, *6*, 866–872.
12. Fontana, M.; Deppe, T.; Boyd, A. K.; Rinzan, M.; Liu, A. Y.; Paranjape, M.; Barbara, P. Electron–Hole Transport and Photovoltaic Effect in Gated MoS_2 Schottky Junctions. *Sci. Rep.* **2013**, *3*, 1634.
13. Bernardi, M.; Palummo, M.; Grossman, J. C. Extraordinary Sunlight Absorption and One Nanometer Thick Photovoltaics Using Two-Dimensional Monolayer Materials. *Nano Lett.* **2013**, *13*, 3664–3670.
14. Ye, Y.; Ye, Z. L.; Gharghi, M.; Zhu, H. Y.; Zhao, M.; Yin, X. B.; Zhang, X. Exciton-Related Electroluminescence from Monolayer MoS_2. *arXiv:1305.4235* [cond-mat.mes-hall] **2013**, *1305*, 4235.
15. Liu, Y. L.; Nan, H. Y.; Wu, X.; Pan, W.; Wang, W. H.; Bai, J.; Zhao, W. W.; Sun, L. T.; Wang, X. R.; Ni, Z. H. Layer-by-Layer Thinning of MoS_2 by Plasma. *ACS Nano* **2013**, *7*, 4202–4209.
16. Mak, K. F.; He, K.; Lee, C.; Lee, G. H.; Hone, J.; Heinz, T. F.; Shan, J. Tightly Bound Trions in Monolayer MoS_2. *Nat. Mater.* **2012**, *12*, 207–211.
17. Newaz, A. K. M.; Prasai, D.; Ziegler, J. I.; Caudel, D.; Robinson, S.; Haglund, R. F., Jr.; Bolotin, K. I. Electrical Control of Optical Properties of Monolayer MoS_2. *Solid State Commun.* **2013**, *155*, 49–52.
18. Tongay, S.; Zhou, J.; Ataca, C.; Liu, J.; Kang, J. S.; Matthews, T. S.; You, L.; Li, J. B.; Grossman, J. C.; Wu, J. Broad-Range Modulation of Light Emission in Two-Dimensional Semiconductors by Molecular Physi-sorption Gating. *Nano Lett.* **2013**, *13*, 2831–2836.
19. Mouri, S.; Miyauchi, Y.; Matsuda, K. Tunable Photoluminescence of Monolayer MoS_2 *via* Chemical Doping. *Nano Lett.* **2013**, *13*, 5944–5948.
20. Qiu, H.; Xu, T.; Wang, Z. L; Ren, W.; Nan, H. Y.; Ni, Z. H.; Chen, Q.; Yuan, S. J.; Miao, F.; Song, F. Q.; *et al.* Hopping Transport through Defect-Induced Localized States in Molybdenum Disulphide. *Nat. Commun.* **2013**, *4*, 2642.
21. Zhou, W.; Zou, X. L.; Najmaei, S.; Liu, Z.; Shi, Y. M.; Kong, J.; Lou, J.; Ajayan, P. M.; Yakobson, B. I.; Idrobo, J. C. Intrinsic Structural Defects in Monolayer Molybdenum Disulfide. *Nano Lett.* **2013**, *13*, 2615–2622.
22. Van der Zande, A. M.; Huang, P. Y.; Chenet, D. A.; Berkelbach, T. C.; You, Y. M.; Lee, G. H.; Heinz, T. F.; Reichman, D. R.; Muller, D. A.; Hone, J. C. Grains and Grain Boundaries in Highly Crystalline Monolayer Molybdenum Disulphide. *Nat. Mater.* **2013**, *12*, 554–561.
23. Komsa, H. P.; Kotakoski, J.; Kurasch, S.; Lehtinen, O.; Kaiser, U.; Krasheninnikov, A. V. Two-Dimensional Transition Metal Dichalcogenides under Electron Irradiation: Defect Production and Doping. *Phys. Rev. Lett.* **2011**, *09*, 035503.
24. Tongay, S.; Suh, J.; Ataca, C.; Fan, W.; Luce, A.; Kang, J. S.; Liu, J.; Ko, C.; Raghunathanan, R.; Zhou, J.; Ogletree, F.; *et al.* Defects Activated Photoluminescence in Two-Dimensional Semiconductors: Interplay between Bound, Charged, and Free Excitons. *Sci. Rep.* **2013**, *3*, 2657.
25. Radisavljevic, B.; Radenovic, A.; Brivio, J.; Giacometti, V.; Kis, A. A. Single-Layer MoS_2 Transistors. *Nat. Nanotechnol.* **2011**, *6*, 147–150.
26. Lee, C.; Yan, H.; Brus, L. E.; Heinz, T. F.; Hone, J.; Ryu, S. Anomalous Lattice Vibrations of Single and Few-Layer MoS_2. *ACS Nano* **2010**, *4*, 2695–2700.
27. Sun, L. F.; Yan, J. X.; Zhan, D.; Liu, L.; Hu, H. L.; Li, H.; Tay, B. K.; Kuo, J. K.; Huang, C. C.; Hewak, D. W.; *et al.* Spin–Orbit Splitting in Single-Layer MoS_2 Revealed by Triply Resonant Raman Scattering. *Phys. Rev. Lett.* **2013**, *111*, 126801.
28. Chakraborty, B.; Bera, A.; Muthu, D. V. S.; Bhowmick, S.; Waghmare, U. V.; Sood, A. K. Symmetry-Dependent Phonon Renormalization in Monolayer MoS_2 Transistor. *Phys. Rev. B* **2012**, *85*, 161403.
29. Mao, N. N.; Chen, Y. F.; Liu, D. M.; Zhang, J.; Xie, L. M. Solvatochromic Effect on the Photoluminescence of MoS_2 Monolayers. *Small* **2013**, *8*, 1312–1315.
30. Gaponenko, M. S.; Lutich, A. A.; Tolstik, N. A.; Onushchenko, A. A.; Malyarevich, A. M.; Petrov, E. P.; Yumashev, K. V. Temperature-Dependent Photoluminescence of PbS Quantum Dots in Glass: Evidence of Exciton State Splitting and Carrier Trapping. *Phys. Rev. B* **2010**, *82*, 125320.
31. Platt, A. D.; Kendrick, M. J.; Loth, M.; Anthony, J. E.; Ostroverkhova, O. Temperature Dependence of Exciton and Charge Carrier Dynamics in Organic Thin Films. *Phys. Rev. B* **2011**, *84*, 235209.
32. Feldmann, J.; Peter, G.; Gobel, E. O.; Dawson, P.; Moore, K.; Foxon, C.; Elliott, R. L. Linewidth Dependence of Radiative Exciton Lifetimes in Quantum Wells. *Phys. Rev. Lett.* **1987**, *58*, 2337.
33. Wirtz, L.; Marini, A.; Rubio, A. Excitons in Boron Nitride Nanotubes: Dimensionality Effects. *Phys. Rev. Lett.* **2006**, *96*, 126104.
34. Wang, S. D.; Chen, Q.; Wang, J. L. Optical Properties of Boron Nitride Nanoribbons: Excitonic Effects. *Appl. Phys. Lett.* **2011**, *99*, 063114.
35. Michler, P.; Hangleiter, A.; Moser, M.; Geiger, M.; Scholz, F. Influence of Barrier Height on Carrier Lifetime in $Ga_{1-y}In_yP/(Al_xGa_{1-x})_{1-y}In_yP$ Single Quantum Wells. *Phys. Rev. B* **1992**, *46*, 7280.

36. Humberto, R. G.; Nestor, P.; Ana, L. E.; Ayse, B.; Wang, B.; Ruitao, L.; Florentino, L. U.; Vincent, H. C.; Humberto, T.; Mauricio, T. Extraordinary Room-Temperature Photoluminescence in Triangular WS_2 Monolayers. *Nano Lett.* **2013**, *13*, 3447–3454.
37. Mahito, Y.; Theodore, L. E.; Michael, S. F.; William, G. C. Anisotropic Etching of Atomically Thin MoS2. *J. Phys. Chem. C* **2013**, *117*, 25643.
38. Skolnic, M. S.; Rorison, J. M.; Nash, K. J.; Mowbray, D. J.; Tapster, P. R.; Bass, S. J.; Pitt, A. D. Observation of a Many-Body Edge Singularity in Quantum-Well Luminescence Spectra. *Phys. Rev. Lett.* **1987**, *58*, 2130.
39. Liu, K. K.; Zhang, W. J.; Lee, Y. H.; Lin, Y. C.; Chang, M. T.; Su, C. Y.; Chang, C. S.; Li, H.; Shi, Y. M.; Zhang, H.; *et al.* Growth of Large-Area and Highly Crystalline MoS_2 Thin Layers on Insulating Substrates. *Nano Lett.* **2012**, *12*, 1538–1544.
40. Brown, N. M. D.; Cui, N. Y.; McKinley, A. An XPS Study of the Surface Modification of Natural MoS_2 Following Treatment in an RF-Oxygen Plasma. *Appl. Surf. Sci.* **1998**, *134*, 11–21.
41. Matioli, E.; Brinkley, S.; Kelchner, K. M.; Hu, Y. L.; Nakamura, S. J.; DenBaars, S.; Speck, J.; Weisbuch, C. High-Brightness Polarized Light-Emitting Diodes. *Light: Sci. Appl.* **2012**, *1038*, 22.
42. Kasim, J.; Yu, T.; You, Y. M.; Liu, J. P.; See, A.; Li, L. J.; Shen, Z. X. Near-Field Raman Imaging Using Optically Trapped Dielectric Microsphere. *Opt. Exp.* **2008**, *16*, 7976–7984.
43. Román-Pérez, G.; Soler, J. Efficient Implementation of a van der Waals Density Functional: Application to Double-Wall Carbon Nanotubes. *Phys. Rev. Lett.* **2009**, *103*, 096102.
44. Kresse, G.; Furthmuller, J. Efficiency of *Ab-Initio* Total Energy Calculations for Metals and Semiconductors Using a Plane-Wave Basis Set. *Comput. Mater. Sci.* **1996**, *6*, 15–51.
45. Klimeš, J.; Bowler, D. R.; Michaelides, A. Van der Waals Density Functionals Applied to Solids. *Phys. Rev. B* **2011**, *83*, 195131.
46. Monkhorst, H. J.; Pack, J. D. Special Points for Brillouin-Zone Integrations. *Phys. Rev. B* **1976**, *13*, 5188–5192.